Journal of Luminescence 145 (2014) 787–792

Contents lists available at ScienceDirect

Journal of Luminescence

journal homepage: www.elsevier.com/locate/jlumin

Expanding broadband emission in the near-IR via energy transfer between Er^{3+}–Tm^{3+} co-doped tellurite-glasses

V.A.G. Rivera [a,b,*], Mohammed El-Amraoui [b], Y. Ledemi [b], Y. Messaddeq [b], E. Marega Jr.[a]

[a] Instituto de Física de São Carlos – INOF, USP, Caixa Postal 369, 13560-970 São Carlos, SP, Brasil
[b] Centre d'optique, photonique et laser, Université Laval, 2375 rue de la Terrasse, G1V 0A6 Quebec (Qc), Canada

ARTICLE INFO

Article history:
Received 11 June 2013
Received in revised form
28 August 2013
Accepted 30 August 2013
Available online 7 September 2013

Keywords:
Tellurite glass
Energy transfer
Optical properties
Broadband emission

ABSTRACT

Processes of energy transfer in Er^{3+}–Tm^{3+} co-doped tellurite glasses has permitted to obtain an expanding broadband emission in the near-infrared region covering the bands S, C+L and U of the optical telecommunications and extending up to the 1700–1900 nm range under excitation by a 976 nm laser diode. This widening of the emission band is achieved through an integrated emission, where the Er^{3+} ions act as donor and the Tm^{3+} ions as acceptor following the route $(Er^{3+})^4I_{11/2} \rightarrow (Tm^{3+})^3H_5$, $(Er^{3+})^4I_{13/2} \rightarrow (Tm^{3+})^3H_4$ and $(Er^{3+})^4I_{13/2} \rightarrow (Tm^{3+})^3F_4$. The relative intensity emission and lifetime of the $^4I_{13/2} \rightarrow {}^4I_{15/2}$ transition of the Er^{3+} ions decrease with increasing the Tm^{3+} concentration. Besides, high Tm^{3+} concentrations produce an emission quenching for the $^3H_4 \rightarrow {}^3F_4$ and $^3F_4 \rightarrow {}^3H_6$ radiative transitions, due to cross-relaxation between Tm^{3+} ions. These effects are studied by means of probability and quantum yield of the energy transfer. The most intense and widest emission band is measured in the glass co-doped with 0.075 and 1 mol% of Tm_2O_3 and Er_2O_3, respectively.

© 2013 Elsevier B.V. All rights reserved.

1. Introduction

Tellurite glasses are convenient host matrix for rare-earth ions (RE) due to their high solubility, high refractive index, low phonon energy (between 700 and 800 cm^{-1}) and extended infrared transmittance [1–3]. From these properties, tellurite glasses appear as good candidate to develop sources with broadband emission in the near-infrared region for applications in the telecommunication window, such as optical amplifiers [4] and low-losses tunable lasers [1]. Today, the Wavelength Division Multiplexing (WDM) in optical communication systems requests a large number of optical carrier signals, which demand a bandwidth as continuous as possible. Nevertheless, it is well known that the emission and amplification of the RE cover separately the O-, E-, S-, C-, L- and U-bands. The enhancement of the amplification bandwidth is thus a current challenge and several approaches have been explored in view to achieve optical amplification covering the entire telecommunication window by: (i) doping glass with metal ions such as Bismuth [5–7] or Nickel [8]; (ii) generating supercontinuum light in highly non-linear optical fiber [9–11] and (iii) co-doping glass with RE ions [12–14]. For the latter, tellurite host glass are usually preferred own to its properties cited above. In glasses co- or triply- doped with RE ions, the energy transfer (ET) processes occurring between the RE ions can either help to improve or decrease its performance (e.g., intensity emission, lifetime) [15]. Hence, ET between two or more RE ions in vitreous systems is extremely important not only from the point of view of applications [14] but also to understand the basic mechanisms [3,16,17]. The efficiency of the ET between a donor–acceptor pair is governed by the Forster mechanism [18] and depends on the distribution function of donor–acceptor distances $f(r)$.

Er^{3+} ions are used for optical amplification processes in C+L-bands due to their $^4I_{13/2} \rightarrow {}^4I_{15/2}$ radiative transition (three levels when pumped at 976 nm) centered around 1530 nm [9,17]. However, the bandwidth and intensity of this emission strongly depends on the host matrix. On the other hand, Tm^{3+} ions exhibit three different emissions in the near-infrared, the $^3H_5 \rightarrow {}^3H_6$ radiative transition of four levels when pumped at 790 nm, the S-band from $^3H_4 \rightarrow {}^3F_4$ radiative indirect transition [18–21] and the $^3F_4 \rightarrow {}^3H_6$ radiative transition in the region 1700–2010 nm [22,23]. Nonetheless, the inversion of population for those electronic transitions is usually difficult to achieve since the short lifetime of the low energy levels can create the so-called "bottelneck" effect. Besides, the broadband emission depends also on the Stark manifolds only for the Er^{3+} and Tm^{3+} ions, which depend on the crystal-field potential. For these reasons, tellurite glasses constitute noble candidates to obtain an integrated emission thanks to an appropriate Er^{3+}–Tm^{3+} ions co-doping and via an ET among the levels $(Er^{3+})^4I_{11/2} \rightarrow (Tm^{3+})^3H_5$, $(Er^{3+})^4I_{13/2} \rightarrow (Tm^{3+})^3H_4$ and $(Er^{3+})^4I_{13/2} \rightarrow (Tm^{3+})^3F_4$ in order to cover the S-, C+L- and U-bands of the optical telecommunications.

* Corresponding author at: Instituto de Física de São Carlos – INOF, USP, Caixa Postal 369, 13560-970 São Carlos, SP, Brasil. Tel.: +55 16 988319159.
E-mail address: garcia@ursa.ifsc.usp.br (V.A.G. Rivera).

0022-2313/$ - see front matter © 2013 Elsevier B.V. All rights reserved.
http://dx.doi.org/10.1016/j.jlumin.2013.08.071

In this work, we propose a co-doped Er^{3+}–Tm^{3+} system which gives a broadband emission of 134 nm width centered at 1534 nm and a broadband emission of 283 nm width centered at 1792 nm in a tellurite glass via an efficient ET process between Er^{3+} and Tm^{3+} ions for a sample doped with 0.075 and 1 mol% of Tm_2O_3 and Er_2O_3, respectively. This process of ET is obtained by pumping directly the Er^{3+} ions with a diode laser at 976 nm, where the luminescence intensity and the lifetime of the $^4I_{13/2} \rightarrow {}^4I_{15/2}$ transition decrease with increasing the Tm^{3+} ions concentration. The most exciting characteristic of the glass system arises from its potential applications as optical fiber amplifier or laser covering the entire telecommunications window.

2. Theoretical considerations

The thermal glass stability against crystallization is usually determined from its characteristic temperatures (glass transition temperature T_g and crystallization temperature T_x) according to: $\Delta T(^\circ C) = T_x - T_g$. The obtained values are reported in Table 1. The concentration N_{RE} in ions/cm^3 of the RE were determined by the equation: $N_{RE} = AN_0\rho/M_{av}$ [24], where A is the RE ions concentration in mol%, N_0 is the Avogadro's number, ρ is the glass density (g/cm^3), and M_{av} is the glass average molecular weight, Table 1.

The residual hydroxyl ion (OH^-) concentration N_{OH} can be estimated from the band centered at 3300 nm in the infrared absorption spectrum by using the Lambert–Beer equation:

$$N_{OH} = \frac{N_0}{\varepsilon_{OH} d} Ln\left(\frac{1}{T}\right) \quad (1)$$

where d is the glass sample thickness and ε_{OH} is the molar absorptivity of free OH^- groups. As no relevant value of ε_{OH} has yet been reported in tellurite glasses, the value $\varepsilon_{OH} = 49.1 \times 10^3$ cm^2/mol determined in silicate glasses has been considered here [25]. Fig. 1(a) shows the corresponding N_{OH} concentrations as a function of Tm^{3+} ions concentration and the glass absorption coefficients at 3300 nm calculated from the transmission spectra as:

$$\alpha_{OH^-} = \frac{Ln(T^{-1})}{d} \quad (2)$$

The interaction between two RE ions can occur via a radiative and/or non-radiative ET in doped glasses [3,14,26,27]. Nevertheless, non-radiative ET processes are dominant in many cases where the interaction between those ions occurs at nearly equal energies between the ground and excited states. This may befall by means of an electric multipole–multipole interaction electric dipole–dipole (dd) or dipole–quadrupole (dq) or quadrupole–quadrupole (qq) type. The probability of non-radiative ET from electric multipolar interactions is given by [28]:

$$W_{NR} = \frac{1}{\tau_{Er^{3+}}} \left(\frac{R_0}{R}\right)^x \quad (3)$$

here, R_0 is the critical distance between two ions at which the non-radiative ET rate becomes equal to the radiative transition rate of the donor, $\tau_{Er^{3+}}$ is the radiative lifetime of the donor. The exponent

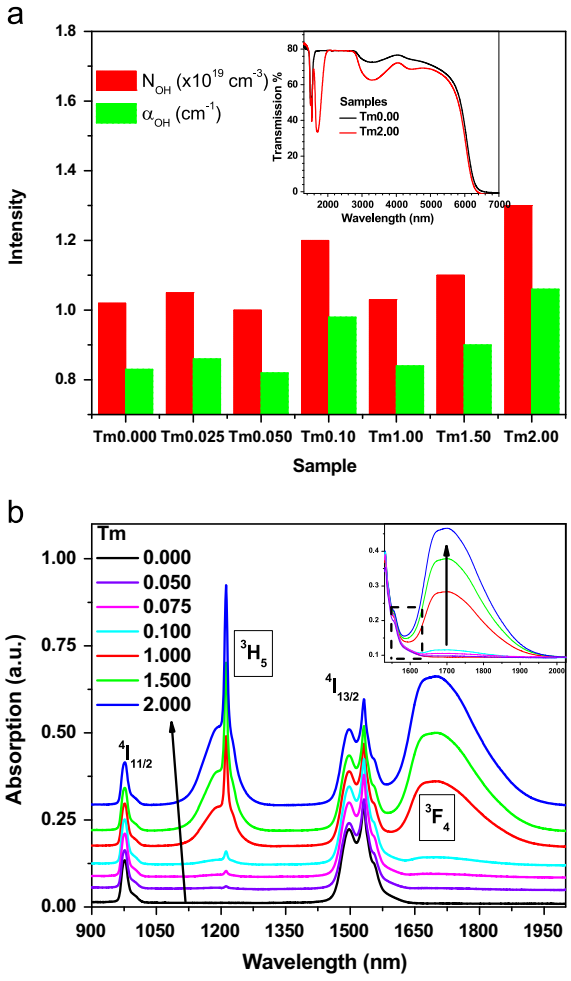

Fig. 1. (a) Linear absorption coefficient α_{OH} at 3300 nm and estimated residual hydroxyl ion concentration in the studied glass samples. Inset: infrared transmission spectra for the Tm0.000 and Tm2.000 samples (thickness: 1 mm). (b) Near-infrared absorption spectra of Er^{3+}–Tm^{3+} tellurite glasses showing the characteristic Er^{3+} and Tm^{3+} absorption bands, with the corresponding absorption transitions from their ground state (framed labels were used for Tm^{3+} levels). The spectra are vertically shifted for a better reading. Inset: increase of the absorption section of Tm^{3+} ions with increasing its concentration in the 1600–2000 nm range.

Table 1
Physical properties of the $74TeO_2$–$10ZnO$–$10Na_2O$–$5GeO_2$–$1Er_2O_3$ glasses as a function of Tm_2O_3 nominal concentration with respective sample labeling used in the text.

Tm_2O_3 (mol%)	Glass sample label	$T_g \pm 2$ °C	$T_x \pm 2$ °C	$\Delta T \pm 4$ °C	$\rho \pm 0.06$ g/cm^3	$N_{Er^{3+}} \pm 0.03 \times 10^y$ ions/cm^3	$N_{Tm^{3+}} \pm 0.03 \times 10^y$ ions/cm^3	Bandwidth (FWHM) centered at (± 3 nm)	
								1535	1793
0.000	Tm0.000	320	491	171	4.95	7.82×10^{22}	0.00	84.9	–
0.025	Tm0.025	317	485	168	5.14	8.11×10^{22}	2.04×10^{21}	79.1	237.9
0.050	Tm0.050	311	486	175	5.15	8.12×10^{22}	4.09×10^{21}	79.1	245.9
0.075	Tm0.075	314	488	174	5.20	8.19×10^{22}	6.20×10^{21}	134.0	283.2
0.100	Tm0.100	319	497	178	5.22	8.22×10^{22}	8.29×10^{21}	92.3	232.6
1.000	Tm1.000	324	527	203	5.23	8.04×10^{22}	8.11×10^{22}	–	239.2
1.500	Tm1.500	322	526	204	5.29	8.03×10^{22}	1.22×10^{23}	–	246.2
2.000	Tm2.000	323	540	217	5.30	7.46×10^{22}	1.51×10^{23}	–	259.8

x is 6, 8 and 10 for the dd, dq and qq interaction, respectively [29]. Let us assume a random distribution of donor and acceptor $f(r)$, with a mean value: $\langle f(r)\rangle = R$ which would be the average distance between donor–acceptor; where R_0 is given by: $R_0 = (3V/4\pi C_0)^{1/3}$, V is the volume of the unit cell of tellurite glass and C_0 is the critical concentration of acceptor, at which the emission intensity of the donor is half of that without acceptor [23]. The ET probability can be then expressed according to [30]:

$$K = \frac{1}{\tau_{Er^{3+}+Tm^{3+}}} - \frac{1}{\tau_{Er^{3+}}} \quad (4)$$

While the quantum yield of ET is given by [31]:

$$\eta = \frac{K\tau_{Er^{3+}}}{1+K\tau_{Er^{3+}}} \quad (5)$$

3. Samples and experimental setup

The host glass composition is $74TeO_2$–$10ZnO$–$10Na_2O$–$5GeO_2$–$1Er_2O_3$ (mol%) and Tm_2O_3 was added at different concentrations from 0.025 to 2.0 mol%, as detailed in Table 1. All the glass samples have been prepared from high purity starting materials (3N and above). The 10 g mixtures were heated in a platinum crucible by using an induction furnace to about 450 °C in order to dry the raw powders for 30 min, and then melted at 760 °C for 1 h under oxidizing conditions by maintaining a low dry oxygen flow within the furnace chamber. Such controlled atmosphere allows in one hand to prevent oxygen losses from tellurite occurring at melting temperature and in the other hand to decrease the OH^- content in the batch, leading to an excellent transparency of glasses in the near-infrared. Afterward, the melted glasses were casted in a pre-heated mold, annealed at 300 °C for 2 h and slowly cooled down to room temperature. Finally, the obtained glass samples were polished up to optical quality required for the optical characterizations.

The thermal properties of the glass samples were examined by differential scanning calorimetry (Netzsch DSC 404F3) in sealed Al pans at a heating rate of 10 °C/min. The density of the samples was measured by the Archimedes method using distilled water as immersion medium and an electronic densimeter MD-300S (Alfa Mirage). The absorption spectra were recorded on a Varian Cary 500Scan UV-VI-NIR double beam spectrophotometer from 900 up to 2000 nm with a resolution of ± 0.3 nm. The relative intensity of OH^- ions (at about 3300 nm) was measured by a Perkin Elmer FT-IR spectrometer Frontier. Steady-state luminescence spectra were obtained from a Nanolog spectrofluorimeter from Horiba Jobin Yvon equipped with a liquid-nitrogen-cooled Symphony InGaAs array near-infrared detector. A pig-tailed diode laser at 976 nm (power 45 mW) was used as external excitation source, by focusing the collimated beam on the sample surface with 18 mm focal lens. The spectral slit width was 12 nm for emission and the acquired data were corrected by instrumental factors.

For the measurements of the $^4I_{13/2}$ excited state lifetime, the samples were excited with a Pico Quant pulsed laser diode laser at 972 nm (model LDH-P-C) with a pulse train of 60 ps and a dead time of 20 ms. Besides, the Xenon flash lamp from the Nanolog system was used as pump source for the 488 and 796 nm excitation wavelengths. The time resolved emission signal centered at 1535 ± 2 nm was measured by a Hamamatsu NIR-PMT module detector coupled to the Nanolog system by employing the method of Time Correlated Single-Photon Counting (TCSPC). Then, a DAS6 decay analysis software was used to obtain the lifetime values through of a single exponential function. Steady-state emission and lifetime measurements were made at room temperature.

4. Results and discussion

Glass samples with good optical quality were prepared. The glass samples present high thermal stability against crystallization, with ΔT values above 160 °C, as seen in Table 1. Besides, T_x and ΔT surprisingly increase with the addition of the Tm^{3+} ions. This confers to these glasses a high potential for optical fiber drawing. Indeed, as fiber drawing is performed above glass transition temperature, the larger is the ΔT value, the lower is the probability that crystallization occurs during the process. And it is well known that the presence of crystals within an optical fiber will dramatically reduce its optical and mechanical properties [32–35].

All the samples were prepared following strictly the same procedure, allowing obtaining glasses with similar infrared transmission spectra as observed in the inset of Fig. 1(a). In these spectra, one can observe one absorption band in the region from 2750 to 3950 nm, which is associated to the stretching vibration of OH^- groups such as $Te(OH)_6$ and H_2TeO_6 [36]. The results of the estimated free OH^- concentrations and absorption coefficients are depicted in Fig. 1(a), where N_{OH} is around $1.10 \pm 0.11 \times 10^{19}$ ions/cm^3 and α_{OH^-} is around 0.90 ± 0.09 cm^{-1}. The obtained values are relatively close for all the samples, showing the good repeatability of the fabrication process. A low N_{OH} in comparison with the $N_{Er}{}^{3+}$ result a short ET rate from the Er^{3+} transition $^4I_{11/2} \rightarrow {}^4I_{13/2}$ toward the OH^- groups (ET_3). The emission intensity from the Er^{3+} ions in these glasses can be thus considered independent from fluctuations of OH^- content. Fig. 1(b) shows the absorption spectra of the prepared samples in the near-infrared region. The absorption bands observed are due to the electronic transitions from the ground state to the Er^{3+} and Tm^{3+} ions excited states, as indicated in Fig. 1(b), by differentiating the Tm^{3+} levels from the Er^{3+} ones with a framed label. The absorption section between 1600 and 2000 nm of the Tm^{3+} ions increases with the increment of the Tm^{3+} ions concentration, see inset Fig. 1(b), while the absorption section of the Er^{3+} ions remains constant.

A spectral feature can be observed between 1590 and 1640 nm, see dot square in the inset Fig. 1(b). It corresponds to an overlap of the absorption bands from the donor (Er^{3+}) and the acceptor (Tm^{3+}) ions, which can be related with the ET process from the expression derived by Dexter [37]. Therefore, this overlap can define the increase of ET process (resonant conditions), which may further increase the emission intensity of the acceptor ion, as observed in the emission spectra presented in Fig. 2(a).

Fig. 2(a) shows the near-infrared emission spectra of the prepared samples under excitation at 976 nm. The emission intensity at 1535 nm (from Er^{3+} ions) decreases for high $N_{Tm}{}^{3+}$ while the emission intensity for the Tm^{3+} bands increases. This is due to the fact that the separation between donor and acceptor ions diminishes when the $N_{Tm}{}^{3+}$ increases, as a result the ET between $(Er^{3+})^4I_{11/2} \rightarrow (Tm^{3+})^3H_5$ and $(Er^{3+})^4I_{13/2} \rightarrow (Tm^{3+})^3F_4$ becomes very efficient, and consequently the emission intensity around 1535 nm decreases. A schematic energy level diagram describing the involved mechanisms is depicted in Fig. 2(b). By pumping at 976 nm, we only observe the $^4I_{13/2} \rightarrow {}^4I_{15/2}$ transition for Er^{3+}-doped, Tm^{3+}-free tellurite glass (Tm0.000), while the $^4I_{13/2} \rightarrow {}^4I_{15/2}$ and $^3F_4 \rightarrow {}^3H_6 + {}^3H_4 \rightarrow {}^3F_4$ transitions are observed for the Er^{3+}–Tm^{3+} co-doped tellurite glasses. In one hand, the Tm0.000 sample exhibits a full width at half maximum (FWHM) of 85 nm for the emission at 1535 nm, covering thus the second part of the S-band (1460–1530 nm) and the entire C-band (1530–1565 nm). On the other hand, the Tm0.075 sample exhibits an emission bandwidth at 1535 nm of 134 nm, covering entirely the S- and C-bands and almost the L-band (1565–1625 nm) besides an emission bandwidth at 1768 nm of 283 nm, ranging from 1627 to 1909 nm and covering thus the U-band (1625–1675 nm). This obtained broadband may also result from the energy splitting of

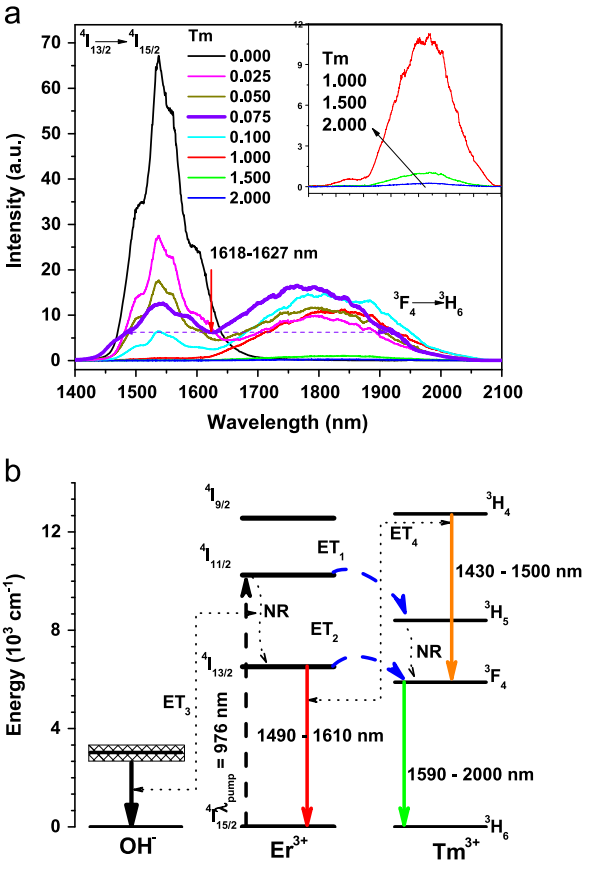

Fig. 2. (a) Near-infrared emission spectra of the Er^{3+}-doped and Er^{3+}–Tm^{3+}-co-doped samples under excitation at 976 nm. The inset shows the emission spectra of the samples with high $N_{Tm}{}^{3+}$. The horizontal dot line highlights the broadband obtained for the Tm0.075 sample. (b) Schematic energy-level diagram with the ET process channels involved between the Er^{3+}, Tm^{3+} and OH^- species proposed to describe the radiative emission bands observed in (a). NR is non-radiative decay.

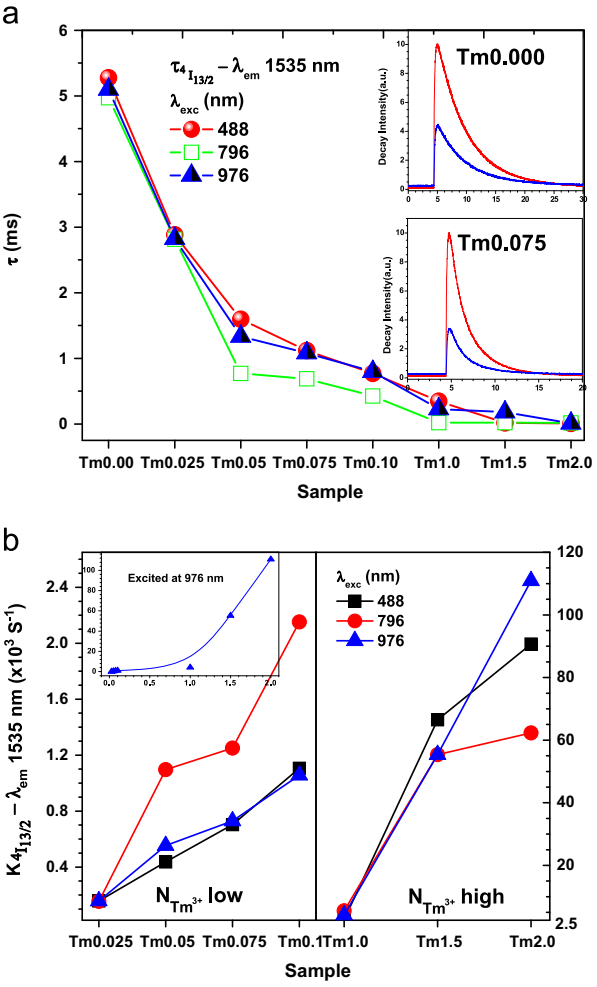

Fig. 3. (a) Lifetime curves at 1535 ± 3 nm monitored under excitation at 488, 796 and 976 nm. Top and bottom insets: decay curves for, respectively, Tm0.000 and Tm0.075 samples excited at 488 and 976 nm. (b) ET Probability (see Eq. (4)) calculated from lifetime measurements, left and right sides for low and high $N_{Tm}{}^{3+}$, respectively. The inset shows the behavior for all samples under the 976 nm excitation.

the Stark levels of each RE ion, Er^{3+} with 7 ($=(2J+1)/2$) and Tm^{3+} with 8 ($=2J+1$), which depend on the multipole interactions between the RE ions and their surroundings, i.e. the ions of the host matrix [38]. The measured FWHM for all the samples are reported in Table 1.

Higher $N_{Tm}{}^{3+}$ induces a decrease in the emission intensity of the Tm^{3+} ions from the Tm1.000 sample, as observed in the inset of Fig. 2(a). This effect can be due to cross-relaxation process where the concentration quenching reduces the quantum efficiency of Tm^{3+} ions. Moreover, this effect can be also attributed to a clustering effect of Tm^{3+} ions, observable at higher ion concentrations [1]. A possible indicator of this cluster formation is the increase of density of the glasses, as reported in Table 1. The involved ET processes are schematically presented in Fig. 2(b). Here, ET processes are starting from the Er^{3+} transitions, explaining the intensity decrease of the Er^{3+} ions emission. Additionally, we must consider ET processes to the residual OH^- groups (ET_3), which is a detrimental process. However, the processes ET_1, ET_2 and ET_4 proposed for this system under excitation at 976 nm make these glasses an active medium that covers entirely the optical communication window.

Fig. 3(a) shows the lifetime measurements of the studied glasses at 1535 nm under excitation at 488, 796 and 976 nm as a function of Tm^{3+} concentration. One can observe that the lifetime of the $^4I_{13/2}$ level decreases drastically in the co-doped glasses when the $N_{Tm}{}^{3+}$ increases up to a fixed $N_{Er}{}^{3+}$, regardless of the excitation wavelength. This result is in agreement with the intensity decrease of the emission band at 1535 nm under excitation at 976 nm, as observed in Fig. 2(a). If we consider that the ET_3 process (multiphoton relaxation rate of the $(Er^{3+})^4I_{11/2}$ level) is constant, we can assume that this drastic decrease is due to ET_2 and ET_4 in which the $^4I_{13/2}$ excited level transfers its energy to the unexcited Tm^{3+} ions populating the $^3H_4$ and $^3F_4$ levels, thanks to a cross-relaxation and multipole interaction, respectively, see Fig. 2(b). Both processes can be expressed as: $(Er^{3+})^4I_{13/2} \rightarrow (Tm^{3+})^3H_4$ and $(Er^{3+})^4I_{13/2} \rightarrow (Tm^{3+})^3F_4$. In order to verify these proposed ET_2 and ET_4, we calculated the ET probability K from the experimental lifetime values, as reported in Fig. 3(b).

For low $N_{Tm}{}^{3+}$, we can observe a subtle increase of the K values in comparison with those observed for high $N_{Tm}{}^{3+}$. The slow increase of ET probability K observed for low $N_{Tm}{}^{3+}$ indicates that the interactions electric dd and electric qd are more favorable in this region since the average distance between donor-acceptor R is inversely proportional to $N_{Tm}{}^{3+}$, Eq. (3). In other words, the Er^{3+} ions are not close enough to Tm^{3+} ions to allow an efficient ET, hence giving low K values.

On the other hand, when $N_{Tm}{}^{3+}$ increases, the average distance R decreases, resulting in high K values where the interaction electric qq type is predominant. This nonlinear behavior is observed for the three excitation wavelengths used here (e.g., inset in Fig. 3(b)). Accordingly, the rapid increase of K also means a rapid decrease of the emission intensity at 1535 nm, which is

verified through the emission spectra presented in Fig. 2(a). Hence, in these glasses, the ET_2 and ET_4 are the predominant processes for the different multipole interactions if compared with the ET_1 and ET_3. Where, ET_1 process increase slowly with the $N_{Tm}{}^{3+}$ increases due the fact that the NR decay $^4I_{11/2}\rightarrow{}^4I_{13/2}$ has higher probability than the ET_1 process $(Er^{3+})^4I_{11/2}\rightarrow(Tm^{3+})^3F_4$, then it increase can stop due cross-relaxation between Tm^{3+} ions.

The quantum yields η (Eq. (5)) of ET between Er^{3+} and Tm^{3+} in the studied glasses as a function of Tm^{3+} concentration are presented in Fig. 4. One can observe that the quantum yield η attains a maximum for high $N_{Tm}{}^{3+}$. Moreover, the critical concentration of acceptor C_0, for which the emission intensity of the donor is half of that without acceptor, was determined for the Tm0.075 sample, giving a quantum yield $\eta=78.2\%$.

Fig. 5(a) compares the normalized absorption and emission spectra of the Tm0.075 sample and the normalized emission spectrum of the Tm0.000 sample. The emission of the Tm0.075 sample exhibits a clear extension of the short wavelength side in comparison to that of Tm0.000 sample. On the other hand, the efficient ET process between donor–acceptor is obtained in Tm0.075 sample from a relative short overlap of about 50 nm of the absorption spectrum, resulting in a broadband of amplified emission in the 1484–1921 nm range with a dark window of about 10 nm width at 1630 nm. Such broad emission could be achieved thanks to an optimal R, i.e., the $N_{Tm}{}^{3+}=C_0$ is sufficient to obtain both efficient ET process and high emission intensity from Er^{3+} and Tm^{3+} ions. Fig. 5(b) is a pictorial representation made from this interpretation showing the mechanism of ET through of the modifiers ions.

The processes mentioned above require a pumping at 976 nm to excite one Er^{3+} ion to the $^3I_{11/2}$ level (see Fig. 2(b)). The increase of emission intensity from the $(Er^{3+})^4I_{13/2}\rightarrow{}^4I_{15/2}$ and $(Tm^{3+})^3F_4\rightarrow{}^3H_6$ radiative transitions must be proportional to the n-th used excitation power laser diode [1], Fig. 6. This way, the peaks intensity at 1535 ± 3 and 1793 ± 3 nm were plotted for the Tm0.075 sample as a function of the pump power in a double logarithmic scale, showing a linear tendency. In both cases a linear behavior starting from an excitation power of 36 mW is observed, giving equal slopes close to 1 for both infrared emissions. This linear increase of the multipole interaction in ET_2:$(Er^{3+})^4I_{13/2}\rightarrow(Tm^{3+})^3F_4$ and ET_4:$(Er^{3+})^4I_{13/2}\rightarrow(Tm^{3+})^3H_4$ results thus from energy transfer process between donor–acceptor.

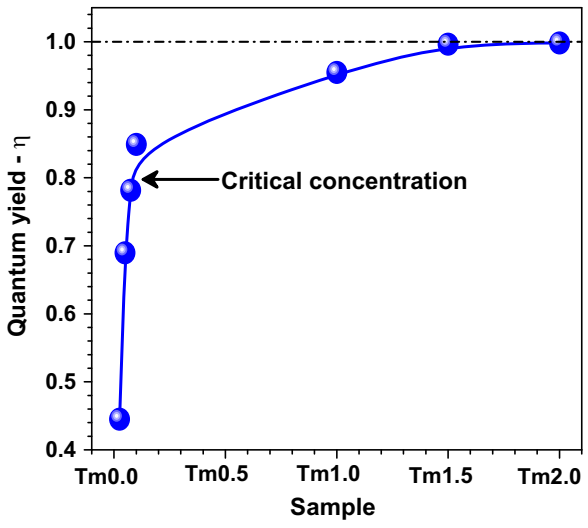

Fig. 4. Quantum yield of ET between Er^{3+} and Tm^{3+} co-doped tellurite glass, values obtained from Eq. (5), when pumped at 976 nm.

5. Conclusions

Er^{3+} and Tm^{3+} co-doped tellurite glasses have been prepared varying the Tm^{3+} ion concentration to investigate their near-infrared

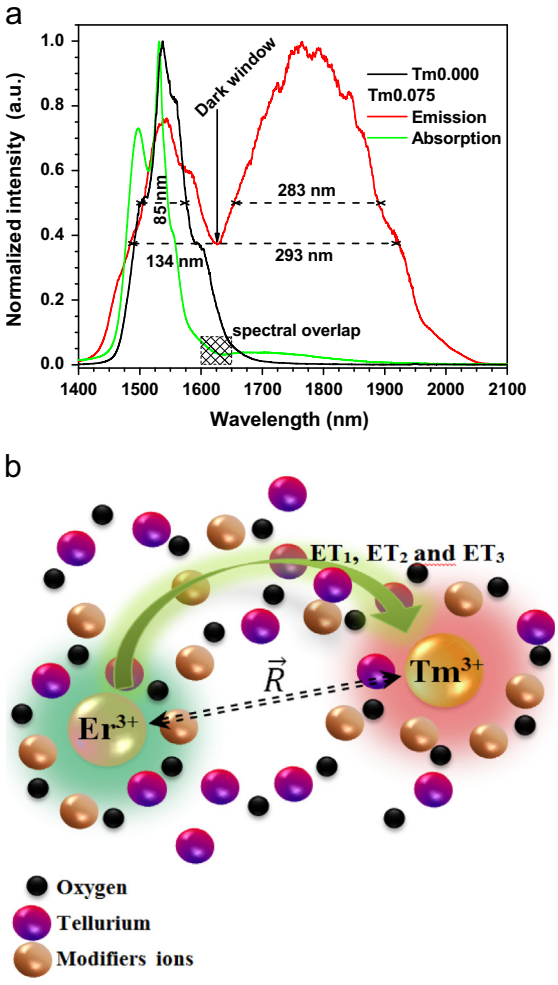

Fig. 5. (a) Normalized absorption and emission spectra of the Tm0.075 sample and normalized emission spectrum of the Tm0.000 sample. The dot line shows the bandwidth (FWHM) for the $^4I_{13/2}\rightarrow{}^4I_{15/2}$, $^3H_4\rightarrow{}^3F_4$ and $^3F_4\rightarrow{}^3H_6$ radiative emissions. The dark window is around 10 nm. (b) Pictorial representation of the surrounding of the REIs into the glass structure, showing the separation distance between donor-acceptor ions and ET_1, ET_2 and ET_3 processes.

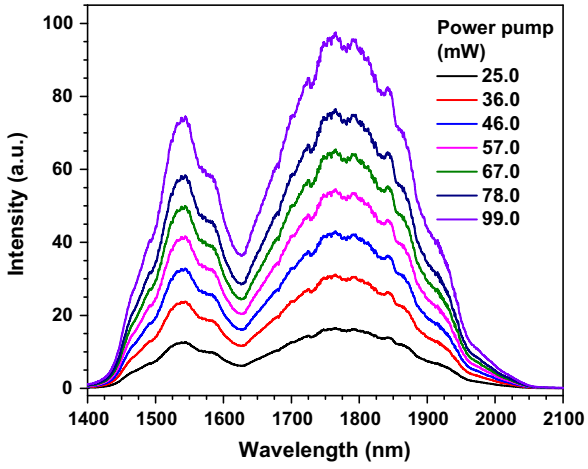

Fig. 6. Emission spectra of the Tm0.075 sample as a function of the pump power from a diode laser at 976 nm.

luminescence. Very good synthesis repeatability was obtained for the studied glasses, allowing maintaining almost constant the low content of free OH^- groups. Besides, these glasses possess a high thermal stability against crystallization. A broadband emission ranging from 1484 to 1921 nm was achieved from the glass co-doped with 1 mol% of Er^{3+} and 0.075 mol% of Tm^{3+} (Tm0.075 sample) under photons absorption at 974 nm. The measured broad emission covers thus the S-, C+L- and U-bands of the optical telecommunication window, with a small dark window of 10 nm, and extends up to 1900 nm. Nonetheless, a decrease of the luminescence intensity and lifetime of $^4I_{13/2}$ level were observed with increasing the Tm^{3+} concentration, due to energy transfers. The bandwidth (FWHM) was increased thanks to the energy transfer process from Er^{3+} to Tm^{3+} ions via $^4I_{13/2} \Longrightarrow^{ET} {}^3H_4, {}^3F_4$ levels, practically with linear behavior for the Tm0.075 sample. On the other hand, high Tm^{3+} concentration resulted in a quenching of the emission via cross-relaxation between Tm^{3+} ions.

Finally, all the near-infrared luminescence features reported in this work, especially for the Tm0.075 sample and its near-infrared emission of 473 nm bandwidth, make these glasses as promising candidates for broadband optical fiber amplifier in the optical communication window and laser sources.

Acknowledgments

This work was supported by the Brazilian agencies FAPESP – Processes: 2009/08978-4 and 2011/21293-0, CNPq through the INOF/CEPOF (Instituto Nacional de Óptica e Fotônica and Centro de Pesquisa em Óptica e Fotônica – São Paulo – Brasil) and the Canadian Excellence Research Chair program (CERC).

References

[1] M.J.F. Digonnet, Rare-Earth-Doped Fiber Lasers and Amplifiers, Marcel Dekker, New York, 1993.
[2] M. Yamane, Y. Asahara, Glasses for Photonics, Cambridge University Press, Cambridge, UK, 2000.
[3] Tripathi Garima, Vineet Kumar Rai, A. Rai, S.B. Rai, Spectrochim. Acta Part A 71 (2008) 486.
[4] V.A.G. Rivera, E. Rodriguez, E.F. Chillcce, C.L. Cesar, L.C. Barbosa, J. Non-Cryst. Solids 353 (2007) 339.
[5] S.F. Zhou, N. Jiang, B. Zhu, H.C. Yang, S. Ye, G. Lakshminarayana, J.H. Hao, J.R. Qiu, Adv. Funct. Mater. 18 (2008) 1407.
[6] X.G. Meng, J.R. Qiu, M.Y. Peng, D.P. Chen, Q.Z. Zhao, X.W. Jiang, C.S. Zhu, Opt. Express 13 (5) (2005) 1628.
[7] Y. Arai, T. Suzuki, Y. Ohishi, S. Morimoto, S. Khonthon, Appl. Phys. Lett. 90 (26) (2007) 261110.
[8] T. Suzuki, Y. Ohishi, Appl. Phys. Lett. 84 (2004) 3804.
[9] B.R. Washburn, S.A. Diddams, N.R. Newbury, J.W. Nicholson, M.F. Yan, C.G. Jorgensen, Opt. Lett. 29 (2004) 250.
[10] K. Saitoh, M. Koshiba, Opt. Express 12 (10) (2004) 2027.
[11] M. El-Amraoui, G. Gadret, J.C. Jules, J. Fatome, C. Fortier, F. Desevedavy, I. Skripatchev, Y. Messaddeq, J. Troles, L. Brilland, W. Gao, T. Suzuki, Y. Ohishi, F. Smektala, Opt. Express 18 (25) (2010) 26655.
[12] L.H. Huang, A. Jha, S.X. Shen, X.B. Liu, Opt. Express 12 (11) (2004) 2429.
[13] S.X. Shen, A. Jha, L.H. Huang, P. Joshi, Opt. Lett. 30 (2005) 1437.
[14] Bo ZhouLili TaoH. Yuen, Tsang Wei Jin, Edwin Yue-Bun Pun, Opt. Express 20 (11) (2012) 12205.
[15] R. Balda, J. Fernández, J.M. Fernández-Navarro, Opt. Express 17 (11) (2009) 8781.
[16] E.F. Chillcce, S.P. Osorio, E. Rodriguez, C.L. Cesar, L.C. Barbosa, Proc. SPIE 5723 (2005) 243.
[17] D. Manzani, Y. Ledemi, I. Skripachev, Y. Messaddeq, S.J.L. Ribeiro, R.E.P. de Oliveira, C.J.S. de Matos, Opt. Mater. Express 1 (8) (2011) 1515.
[18] K.A.Gschneider, Jr., J.C.G. Bunzli, V.K. Pecharsky, Handbook on the Physics and Chemistry Rare Earths: Optical Spectroscopy, vol. 41, 2011, Elsevier, The Netherlands, Oxford OX5 IGB, UK.
[19] R. Rolli, M. Montagna, S. Chaussedent, A. Monteil, V.K. Tikhomirov, M. Ferrari, Opt. Mater. 21 (2003) 743.
[20] S. Tanabe, T. Tamaoka, J. Non-Cryst. Solids 326–327 (2003) 283.
[21] M. Shi Qing, W. Sun Fat, E.Y.B. Pun, C. Po Shuen, J. Opt. Soc. Am. B 21 (2) (2004) 313.
[22] Milanese Daniel, Monica Vota, Qiuping Chen, Jianjun Xing, Guihua Liao, Hrvoje Gebavi, Monica Ferraris, Nicola Coluccelli, Stefano Taccheo, J. Non-Cryst. Solids 354 (2008) 1955.
[23] Wu Jianfeng, Zhidong Yao, Jie Zong, Shibin Jiang, Opt. Lett. 32 (2007) 638.
[24] V.A.G. Rivera, S.P.A. Osorio, D. Manzani, Y. Messaddeq, L.A.O. Nunes, E. Marega Jr., Opt. Mater. 33 (2011) 888.
[25] X. Feng, S. Tanabe, T. Hanada, J. Non-Cryst. Solids 281 (1–3) (2001) 48.
[26] P.R. Biju, G. Jose, V. Thomas, V.P.N. Nampoori, N.V. Unnikrishnan, Spectrochim. Acta Part A 71 (2008) 486.
[27] Zhaogang Nie, Ki-Soo Lim, Jiahua Zhang, Xiaojun Wang, J. Lumin. 129 (2009) 844.
[28] J.R. Lakowicz, Principles of Fluorescence Spectroscopy, 2nd ed., Plenum Press, New York, 1999. (Springer).
[29] Yong Beom Shin, Jong Heo, J. Non-Cryst. Solids 256–257 (1999) 260.
[30] A. Braud, S. Girard, J.L. Doualan, M. Thuau, R. Moncorge, A.M. Tkachuck, Phys. Rev. B 61 (8) (2000) 5280.
[31] P.R. Biju, G. Jose, V. Thomas, V.P.N. Nampoori, N.V. Unnikrishnan, Opt. Mater. 24 (2004) 671.
[32] P.G. Debenedetti, H.E. Stanley, Phys. Today 56 (6) (2003) 40.
[33] A. Lin, A. Zhang, E.J. Bushong, J. Toulouse, Opt. Express 17 (19) (2009) 16716.
[34] S.P.A. Osorio, V.A.G. Rivera, D. Manzani, L.A.O. Nunes, Y. Messaddeq, E. Marega Jr., Plasmonics 7 (1) (2012) 53.
[35] Xuming Wang, Spectrochim. Acta Part A 70 (2008) 99.
[36] Dai Shixum, Chunlei Yu, Gang Zhou, Junjie Zhnag, Guonian Wang, Lili Hu, J. Lumin. 117 (2006) 39.
[37] D.L.A. Dexter, J. Chem. Phys. 21 (1953) 836.
[38] Y.D. Huang, M. Mortier, F. Auzel, Opt. Mater. 15 (2001) 243.